Experimental and Numerical Study of the Laminar Burning Velocity of Biogas–Ammonia–Air Premixed Flames

Pierre Brequigny, Adnane Soulé, Christine Mounaïm-Rousselle, Guillaume Dayma, Fabien Halter

energies

MDPI

Article

Experimental and Numerical Study of the Laminar Burning Velocity of Biogas–Ammonia–Air Premixed Flames

Pierre Brequigny [1,*], Adnane Soulé [1], Christine Mounaïm-Rousselle [1], Guillaume Dayma [2] and Fabien Halter [2]

[1] PRISME, University Orléans, INSA-CVL, F-45072 Orléans, France
[2] CNRS-ICARE, University Orléans, F-45072 Orléans, France; fabien.halter@cnrs-orleans.fr (F.H.)
* Correspondence: pierre.brequigny@univ-orleans.fr

Abstract: Biogas is a gas resulting from the digestion of biomass, which means transforming organic waste into energy. It is composed essentially of methane (CH_4) and carbon dioxide (CO_2) and can also contain ammonia (NH_3) as an impurity. Biogas is generally used to generate electricity or produce heat in a cogeneration system. With the renewed interest in ammonia and the increasing development of biogas caused by the urge for an energetic transition, those two carbon-neutral fuels are being investigated as a mixture in this study through the laminar burning velocity (LBV). In this paper, the LBV of biogas ammonia air mixtures are investigated experimentally for the first time over a wide range of equivalence ratios and ammonia concentrations. The biogas studied was 60% CH_4 and 40% CO_2 in volume. The NH_3 concentration in the fuel varied from 0 to 50% vol. while the equivalence ratio varied from 0.8 to 1.2. The experiments were conducted at constant pressure in a constant volume vessel at 300 K and 1 bar. Adding ammonia to biogas decreases the LBV while the Markstein length is not very sensitive to ammonia addition. The CEU-NH3-Mech-1.1 and Okafor mechanisms show good agreement with the experimental laminar burning velocity. The effect of radiative heat losses on the measurement is also investigated.

Keywords: biogas; ammonia; premixed combustion; laminar burning velocity

Citation: Brequigny, P.; Soulé, A.; Mounaïm-Rousselle, C.; Dayma, G.; Halter, F. Experimental and Numerical Study of the Laminar Burning Velocity of Biogas–Ammonia–Air Premixed Flames. *Energies* **2024**, *17*, 319. https://doi.org/10.3390/en17020319

Academic Editors: Clara Mendoza Martinez, Esa Kari Vakkilainen, Elem Patricia Alves Rocha and Wei-Hsin Chen

Received: 27 October 2023
Revised: 14 December 2023
Accepted: 27 December 2023
Published: 9 January 2024

1. Introduction

The need for alternative fuels is strongly dependent on pressures applied by society and government policies. Biomass continues to be the main renewable energy source in Europe and is considered to be one of the solutions to achieve the EU energy targets for 2030 [1]. Among biomass energy types, biogas is an alternative fuel easily produced from various feedstocks such as crop residues, organic wastes, sewage sludge or landfills [2–4]. Biogas is mainly composed of CH_4 (50–70%vol.) and CO_2 (30–50%) but can contain traces of N_2, O_2 and several impurities such as H_2S or NH_3. Ammonia can appear as an impurity when the feedstock used for anaerobic digestion is nitrogenous-rich such as manure or sewage sludge. Moreover, ammonia has recently gained a renewed interest as a potential zero-carbon fuel in internal combustion engines especially in spark-ignition (SI) ones. Indeed, despite his unfavorable combustion properties [5], stable operation was achieved with neat ammonia in SI engines with different architectures [6–8]. It could also be noticed that one of the first uses of ammonia in engines dates back to WWII in Belgium, where the bus fleet operated with the first dual-fuel engine ever reported: coal gas (syngas) composed of 50% H_2 directly injected in the combustion chamber filled with ammonia [9]. In order to predict and improve the performance of practical combustion systems, key parameters of the combustion process must be determined beforehand. One important parameter is the laminar flame speed, S_L^0, of the fuel air mixture, which indicates its usability under certain engine operating conditions or its propensity to flashback in burners. The knowledge of this parameter is even crucial for the CFD simulation of an engine or a gas turbine since the turbulent flame development in such devices is directly related to S_L^0. Two ways

could be used to compute this parameter under real conditions: either with a correlation proposed from the experimental database as a function of blends and conditions or with a kinetic mechanism previously validated against experimental S_L^0 values in order to model a practical combustion system. The Markstein length, L_b, is another measurable parameter that characterizes the flame response to stretch, influenced by thermal and mass diffusivities whose ratio is the Lewis number. This parameter is of importance for understanding the flame dynamics in practical combustion systems such as gas turbines or engines where turbulence affects the flame front development or propagation differently depending on the Lewis number and the Markstein length. L_b and S_L^0 can both be determined experimentally using the spherical expanding flame technique at constant pressure.

Data on the laminar flame speed of biogas are rather limited in the literature. Nonaka et al. [10] investigated the effect of the CO_2 content on the laminar flame speed using the heat flux burner. They showed a decrease in the laminar flame speed when increasing the CO_2 content from 0 to 50% in volume at 1 bar and 298 K, mainly due to a thermal (i.e., decrease in the adiabatic flame temperature). Similarly for pure CH_4, the maximum flame speed is reached for an equivalence ratio about 1 to 1.1 no matter the composition of the biogas. Hinton and Stone [11] used the constant volume hypothesis to measure the laminar flame speed of biogas with up to 40% CO_2 for a wide range of temperature and pressure conditions and proposed a correlation as a function of equivalence ratio, pressure, temperature, and CO_2 content. More recently, Wei et al. investigated the possibility to increase the laminar flame speed of biogas by adding hydrogen to the blend [12].

Regarding ammonia, recent experimental studies have investigated S_L^0 and L_b characteristics, notably Hayakawa et al. [13] from atmospheric to 5 bar of initial pressure and Kanoshima et al. [14], who extended the work to include the influence of initial temperature. The influence of temperature as well as hydrogen addition were also investigated by Lhuillier et al. [5]. Results from these works highlight that S_L^0 peaks at an equivalence ratio ϕ of ≈ 1.1, with an increase in pressure and temperature resulting in a decrease and increase in S_L^0, respectively. Concerning L_b, NH_3/air flames show an increasing L_b trend with increasing ϕ, similar to CH_4/air and H_2/air flames. It is worth noting that at normal temperature and pressure conditions (T = 298 K, P = 0.1 MPa), lean NH_3 flames exhibit negative L_b, while positive values are observed at rich conditions. Those results were updated and analyzed in depth recently by Zitouni et al. [15] showing the importance of fundamental parameters such as the Lewis number, the expansion ratio, and the activation energy, i.e., the Zel'dovich number in the stretch response.

To the best of the author's knowledge, there is currently no study investigating the fundamental combustion properties of blends of biogas and ammonia. Mong et al. [16] recently investigated the use of such a blend but in a swirled burner, showing that the use of biogas instead of neat methane in the methane/ammonia blend is expected to increase the turbulent intensity compared to the laminar flame speed. This phenomenon will intensify as ammonia content is increased in the blend especially for NH_3 > 40%vol in the ammonia/biogas blend. Concerning laminar flame speeds, ammonia methane blends (but without CO_2) were recently deeply investigated in the literature [15,17–21]. Those studies showed very similar results despite the use of different measurement techniques such as heat flux burner, constant volume, or constant pressure spherical expanding flames. Due to the very low reactivity of ammonia and its very low flame speed (about 6–8 cm/s at ambient conditions), blending it with methane results in a decrease in the flame speed of CH_4. For instance, the flame speed of methane at ambient conditions peaks at 36–38 cm/s whereas it does not exceed 19–20 cm/s for 50/50 NH_3/CH_4 blends.

The objective of the present work is therefore to provide laminar flame speed and Markstein length of biogas/ammonia blends using the constant pressure spherical expanding flame methodology. For this purpose, a 60% CH_4/40% CO_2 blend, called biogas 60/40 was used to represent biogas and mixed with ammonia up to 50%vol. in the fuel blend. The equivalence ratio varied from 0.8 to 1.2. Results were compared with different kinetic mechanisms, and radiative effects were discussed.

2. Materials and Methods

2.1. Laminar Flame Speed Measurment

The laminar flame speed setup used here consists of an optically accessible 4.2 L constant volume spherical vessel in which a series of flowmeters is used to simulate different mixture compositions. A high-speed Schlieren setup is used to obtain images of the propagating flame and determine the laminar burning velocity using the constant pressure methodology. This setup is described in depth in the following work [5]. A schematic view of the setup is displayed in Figure 1.

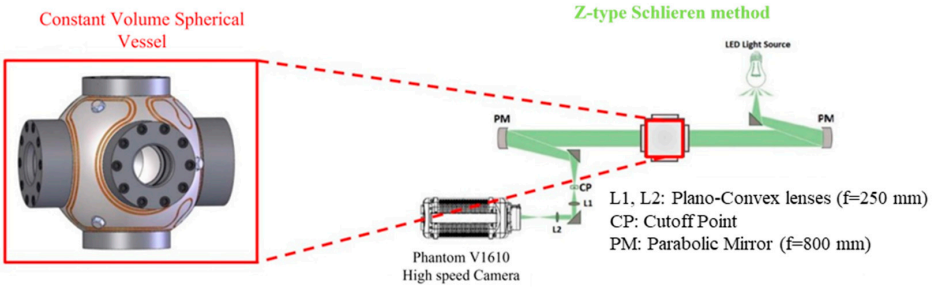

Figure 1. Schematic view of the setup.

The vessel has four 70 mm diameter quartz windows. A vacuum pump is connected to the vessel to ensure that the pressure at the beginning of the filling process is below 10 mbar. Three gaseous flowmeters deliver the air/biogas/ammonia. The 60/40 biogas blend was prepared in the premixed bottle using a Coriolis mass flowmeter using the partial pressure method. The partial pressure was checked at the end of the introduction of each component to be equal to the desired quantity with less than a 3% deviation. To ensure homogeneity in the biogas bottle, a fan is switched on before the introduction into the spherical vessel and keeps running during the injection of the gas in the spherical vessel. Moreover, another fan rotates in the spherical vessel during the filling process guaranteeing homogeneity of the mixture and is stopped 20 s before the spark to avoid any turbulent motion during combustion. Several heating elements are placed along the intake line and on the vessel itself (as shown by the incrusted orange wires in Figure 1) and the temperature inside the vessel is controlled by k-type thermocouples. The ignition system consists of an automotive coil-on-plug device connected to two 0.5 mm thick electrodes with a 1.5 mm gap between them. Coil charge duration was set to have the minimum discharge energy allowing ignition and propagation. A high-speed Phantom V1610 camera from Vision Research/AMETEK is used for image acquisition, set at 7000 frames per second with a spatial resolution of 0.11 mm/pixel. The post-processing is performed in the MATLAB R2022b environment and consists of obtaining the flame contour and equivalent radius as a function of time. First, the background is subtracted, then images are binarized, and spatially filtered using a low-pass filter to reduce noise on the contour of the flame front. The radius corresponding to this contour is given by Equation (1).

$$R_f = \sqrt{\frac{A}{\pi}}, \tag{1}$$

where A, is the flame area. The flame speed, S_b, and stretch, K, profiles are then calculated as follows:

$$S_b = \frac{dR_f}{dt}; \; K = \frac{2}{R_f} S_b \tag{2}$$

The non-linear extrapolation method is used to provide the unstretched flame speed value, S_b^0, and the Markstein length using Equation (1)

$$\left(\frac{S_b}{S_b^0}\right)^2 \ln\left(\frac{S_b}{S_b^0}\right)^2 = -\frac{2L_b K}{S_b^0} \tag{3}$$

Finally, the unstretched laminar burning velocity, S_L^0, is given by $S_L^0 = \frac{\rho_b}{\rho_u} S_b^0$ with ρ_b and ρ_u respectively the burned and unburned densities calculated using the equilibrium routine of ANSYS CHEMKIN Pro.

The uncertainties presented are calculated based on the work of Moffat [22] and were detailed in previous works [5]. Overall uncertainty values are the combination of statistical, hardware-related (3.5% due to pressure and temperature) and imaging (2.5%) errors. Statistical errors are defined as $\Delta S_L^0 / S_L^0 = t_{95\%} \cdot \sigma_{std} / \sqrt{N}$ where σ_{std} is the standard deviation and $t_{95\%}$ is the value of the Student's law for N = 3 tests in a 95% confidence interval. The uncertainties in the mixture composition are due to the accuracy of the mass flow meters (1% of the full scale), resulting in a maximum uncertainty of 3% in the target equivalence ratio. Measurements were made at 1 bar absolute initial pressure and the initial temperature was 300 ± 3 K. For the present study, a biogas with 40%vol. CO_2 and 60%vol. CH_4 was selected. The volume fraction of NH_3 in the biogas/NH_3 blend was varied as follows: 5, 10, 15, 25, and 50%vol.

2.2. Kinetics Simulation Setup

Numerical simulations were carried out using the premixed laminar flame-speed calculation module of ANSYS CHEMKIN-PRO 2020 R1 to estimate the laminar flame speed and assess the validity of several chemical kinetic mechanisms. The maximum number of grid points was set to 1000 with 50 adaptative grid points. GRAD and CURV parameters were set to 0.1 and 0.05 respectively. The length of the domain was set to 10 cm. Since ammonia presents very different diffusive properties compared to conventional fuels [15] the Soret effect was considered in order to account for those phenomena as in many studies dealing with ammonia [23], hydrogen [24], or multi-component fuel [25] similarly to the present work, and a mixture averaged transport model was used. Four mechanisms, displayed in Table 1, containing the required species, were first tested on pure biogas and CH_4/NH_3 blends to select the most suitable before validation on biogas/ammonia blends.

Table 1. Selected chemical kinetic mechanisms.

Mechanism	Type	Number of Species	Number of Reactions
Okafor [18] (2018)	Reduced	42	130
Shrestha [26] (2018)	Detailed	125	1090
CEU-NH3-Mech-1.1 [21] (2022)	Detailed	91	444
San Diego [27]	Reduced	69	311

3. Results

3.1. Mechanisms Validation

Simulation results were compared to the experimental data of Nonaka and Pereira [10], Wei et al. [12] and Nurmukan et al. [28] at ambient conditions in Figure 2. The bar graph shows overall good agreement between simulations and experiments with better performances for Okafor and CEU-NH3-Mech-1.1. The San Diego mechanism also performs well around stoichiometry but shows higher discrepancies with experiments on the lean and rich sides. The mechanisms were also compared to the dataset of Hinton and Stone [11] at higher pressures, namely 2 and 4 bar, with three different temperatures 298, 380 and 450 K leading to the same conclusions as with ambient conditions. At this stage, the Shrestha mechanism is no longer considered due to its higher discrepancies.

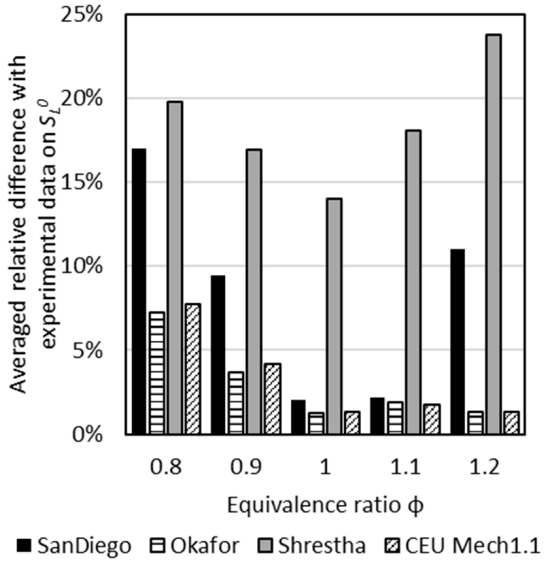

Figure 2. The relative difference between simulations and averaged experimental laminar burning velocities for biogas 60/40 at 1 bar and 300 ± 3 K [10,12,28].

To assess the prediction of the mechanism with ammonia, simulations were compared with experimental data of various CH_4/NH_3 blends from Wang et al. [21] and Han et al. [20] at 1 atm and 298 K. This comparison is presented in Figure 3. The mechanisms show overall good agreement with the experiments in the literature. Yet the San Diego mechanism shows higher differences on the lean side with a low ammonia content. Results were akso compared at higher pressure with the experiments of Okafor et al. [19], Wang et al. [21], and Shu et al. [17]. An extensive comparison between the available literature data for ammonia/methane blends and the Okafor, San Diego and CEU-NH3-Mech-1.1 mechanisms is presented in Table 2, Table 3, and Table 4, respectively. As a result, only Okafor and CEU-NH3-Mech-1.1 were retained for the remainder of the study since they showed the best agreement with the experimental data in the literature.

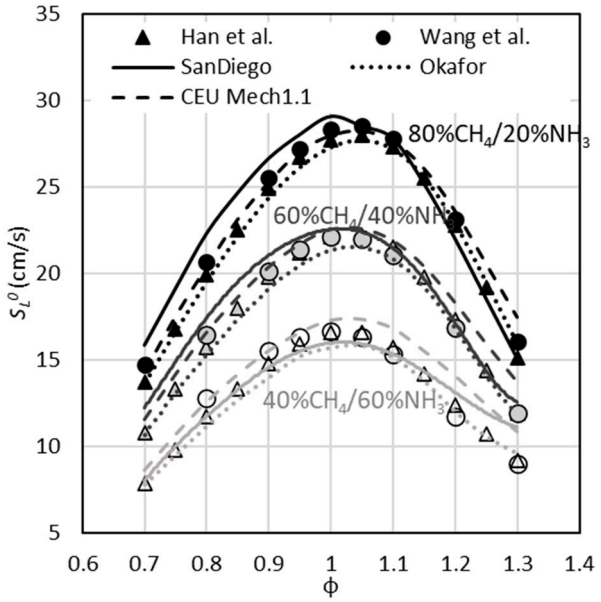

Figure 3. Laminar burning velocities of CH_4/NH_3 blends. Comparison of mechanisms with data from Han et al. [20] and Wang et al. [21] at 1 bar and 300 ± 3 K. Black, grey and white symbols respectively represent the $80\%CH_4/20\%NH_3$, $60\%CH_4/40\%NH_3$ and the $40\%CH_4/60\%NH_3$ blends.

Table 2. Relative differences between experimental laminar burning velocities available in the literature and the Okafor mechanism for the CH_4/NH_3 blend. The values are colored with a gradient from green (low differences) to red (high differences).

φ	1 atm 298 K [21]			1 atm 298 K [22]			3 atm 298 K [22]			5 atm 298 K [22]			1 atm 298 K [18]			5 atm 298 K [18]			3 bar 298 K [20]			5 bar 298 K [20]			Min	Max	Avg.
	%NH_3			%NH_3			%NH_3			%NH_3			%NH_3			%NH_3			%NH_3			%NH_3					
	20	40	60	20	40	60	20	40	60	20	40	60	10	50	90	10	50	90	22	39	52	22	39	52			
0.7	0.0%	1.0%	0.9%	7.1%			10.3%	15.3%		15.3%	24.4%		19.1%	21.5%											0.0%	24.4%	11.5%
0.8	1.6%	2.5%	4.2%	5.2%	7.0%	12.5%	6.9%	11.4%	10.9%	8.2%	13.6%	14.1%	4.8%	9.3%		9.8%	23.0%	11.2%	6.0%	7.8%	7.6%	1.9%	4.3%	7.3%	1.6%	23.0%	8.3%
0.9	1.9%	3.6%	5.4%	4.4%	5.3%	9.7%	5.6%	8.4%	8.1%	7.0%	7.5%	5.4%	5.3%	6.4%				17.0%	1.3%	0.5%	2.3%	3.9%	1.4%	5.4%	0.5%	17.0%	5.5%
1	1.4%	3.5%	5.4%	3.6%	3.5%	5.7%	5.2%	8.2%	9.8%	5.8%	7.3%	4.9%	3.0%	0.1%	13.4%	3.0%	0.9%	13.7%	0.1%	0.8%	0.6%	3.9%	2.0%	1.9%	0.1%	13.7%	4.5%
1.1	0.5%	3.1%	3.6%	2.3%	1.1%	1.1%	3.3%	8.0%	9.6%	0.4%	3.5%	1.4%	1.1%	3.3%	0.8%			7.8%	0.6%	2.5%	1.6%	2.8%	2.2%	2.3%	0.4%	9.6%	2.9%
1.2	0.3%	3.0%	3.2%	1.0%	0.5%	2.2%	9.3%	15.0%	9.0%	3.9%	4.0%	7.7%	3.0%	5.8%	14.1%	5.7%	3.0%	0.8%	6.6%	7.7%	3.4%	8.6%	4.9%	2.0%	0.3%	15.0%	5.2%
1.3	5.6%	0.1%	4.4%	0.7%	0.4%	6.7%	11.8%	6.7%	5.1%	0.6%	10.0%	35.8%	9.7%	5.3%	38.6%			2.9%	8.1%	0.6%	1.9%	2.1%	6.3%	10.8%	0.1%	38.6%	7.9%

Table 3. Relative differences between experimental laminar burning velocities available in the literature and the San Diego mechanism for the CH_4/NH_3 blend. The values are colored with a gradient from green (low differences) to red (high differences).

φ	1 atm 298 K [21]			1 atm 298 K [22]			3 atm 298 K [22]			5 atm 298 K [22]			1 atm 298 K [18]			5 atm 298 K [18]			3 bar 298 K [20]			5 bar 298 K [20]			Min	Max	Avg.
	%NH_3			%NH_3			%NH_3			%NH_3			%NH_3			%NH_3			%NH_3			%NH_3					
	20	40	60	20	40	60	20	40	60	20	40	60	10	50	90	10	50	90	22	39	52	22	39	52			
0.7	15.9%	13.4%		7.7%			3.6%	4.3%		0.6%	13.9%		35.6%	34.1%											0.6%	35.6%	14.3%
0.8	12.2%	10.5%		8.1%	5.5%		3.3%	2.4%	7.5%	1.0%	5.5%	10.0%	17.1%	19.9%	2.9%	18.3%	32.1%	3.0%	17.8%	19.0%	15.0%	12.4%	14.3%	14.7%	1.0%	32.1%	11.5%
0.9	7.0%	6.1%	1.5%	4.3%	4.3%	5.9%	0.8%	2.9%	5.9%	3.7%	2.9%	3.0%	12.5%	15.1%	3.4%			10.0%	6.8%	6.7%	6.7%	0.6%	3.1%	9.3%	0.6%	15.1%	5.6%
1	4.9%	2.0%	4.0%	2.5%	2.0%	4.3%	5.9%	7.7%	9.0%	10.3%	8.3%	4.1%	5.9%	4.1%	1.1%	10.6%	0.8%	13.3%	1.1%	0.2%	1.3%	8.0%	3.2%	2.7%	0.2%	13.3%	4.9%
1.1	1.8%	0.3%	1.8%	0.0%	2.5%	0.8%	10.5%	9.5%	4.7%	11.0%	4.4%	10.9%	2.2%	0.2%	4.7%				7.3%	4.5%	0.6%	12.2%	3.6%	1.5%	0.0%	12.2%	4.5%
1.2	3.5%	1.5%	5.0%	4.7%	1.1%	10.8%	17.4%	11.9%	4.8%	12.3%	1.4%	26.2%	8.7%	2.0%	28.6%	20.8%	15.2%	20.9%	13.1%	5.1%	7.2%	15.3%	0.4%	10.7%	0.4%	28.6%	10.3%
1.3	0.1%	5.7%	20.6%	5.8%	5.2%	23.3%	12.7%	2.2%	26.5%	0.3%	21.2%	64.0%	19.5%	4.8%	62.7%				7.5%	9.1%	18.5%	1.1%	16.4%	30.1%	0.1%	64.0%	17.0%

Table 4. Relative differences between experimental laminar burning velocities available in the literature and the CEU-NH3-Mech-1.1 mechanism for the CH_4/NH_3 blend. The values are colored with a gradient from green (low differences) to red (high differences).

φ	1 atm 298 K [21]			1 atm 298 K [22]			3 atm 298 K [22]			5 atm 298 K [22]			1 atm 298 K [18]			5 atm 298 K [18]			3 bar 298 K [20]			5 bar 298 K [20]			Min	Max	Avg.
	%NH_3			%NH_3			%NH_3			%NH_3			%NH_3			%NH_3			%NH_3			%NH_3					
	20	40	60	20	40	60	20	40	60	20	40	60	10	50	90	10	50	90	22	39	52	22	39	52			
0.7	4.3%	6.9%	9.2%	3.1%			1.9%	5.5%		2.8%	14.8%		22.1%	33.0%											1.9%	33.0%	10.3%
0.8	2.5%	5.7%	7.6%	1.3%	0.9%	1.6%	0.4%	2.1%	1.5%	1.3%	4.1%	7.3%	8.0%	19.1%		19.7%	35.3%	4.0%	14.5%	18.9%	19.5%	13.0%	15.8%	17.7%	0.4%	35.3%	9.7%
0.9	1.5%	3.0%	5.2%	1.1%	1.2%	0.4%	0.5%	0.2%	1.0%	0.7%	0.6%	1.4%	8.1%	16.2%				10.3%	8.1%	10.0%	12.6%	2.9%	7.1%	14.3%	0.2%	16.2%	5.1%
1	1.0%	2.1%	4.4%	1.3%	2.1%	4.1%	2.3%	1.8%	1.4%	1.9%	1.3%	1.7%	4.8%	7.6%	18.4%	1.5%	8.1%	10.0%	3.5%	5.9%	9.5%	0.4%	4.3%	10.0%	0.4%	18.4%	4.6%
1.1	1.3%	1.9%	7.3%	0.5%	4.1%	10.1%	0.4%	0.1%	2.9%	2.0%	4.7%	12.7%	0.2%	4.5%	11.1%			18.4%	2.9%	4.6%	10.3%	0.2%	4.9%	7.6%	0.1%	18.4%	5.1%
1.2	3.6%	5.9%	13.8%	2.3%	8.7%	20.1%	2.8%	2.7%	6.3%	1.9%	7.0%	21.4%	0.7%	7.8%	28.6%	3.3%	15.9%	7.1%	0.6%	5.4%	11.7%	2.4%	6.0%	10.4%	0.6%	28.6%	8.2%
1.3	15.7%	15.4%	18.1%	8.9%	14.9%	20.8%	3.9%	2.4%	14.4%	4.5%	15.3%	44.0%	3.9%	8.2%	50.4%			8.3%	1.0%	8.4%	11.1%	1.9%	11.5%	17.1%	1.0%	50.4%	13.6%

3.2. Experimental Laminar Burning Velocities

As per validation, Figure 4 shows the comparison of the laminar flame speeds S_L^0 of the present work with previous experiments of Nonaka and Pereira [10], Wei et al. [12] and Nurmukan et al. [28], as well as with the two selected mechanisms for biogas only. All the reported data, experimental or numerical, fall within the uncertainty of the present work.

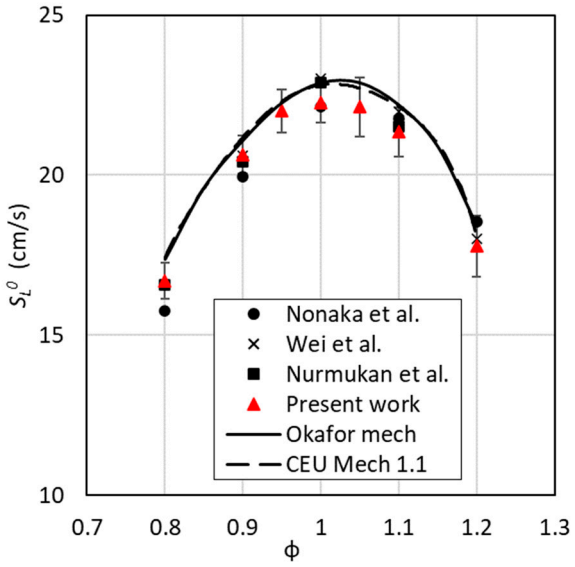

Figure 4. Comparison of biogas/air laminar flame speeds results at 1 bar and 300 ± 3 K with previous experimental data of Nonaka and Pereira [10], Wei et al. [12] and Nurmukan et al. [28] and the selected mechanisms.

Figure 5 shows examples of flame images at ϕ = 1.0 for various ammonia content 16 ms after ignition. It can be seen that for all NH_3 contents the flame remains spherical and does not seem to be affected by any instability, such as buoyancy, which has been observed for a neat ammonia flame [14,15]. The decrease in the flame speed with the addition of NH_3 is also visible since the flame diameter decreases at the same time when adding NH_3 to the blend. Experiments were also conducted at 75% of NH_3, but due to less contrast, local extinction, and the appearance of buoyancy instabilities, it was not possible to process the images, especially for rich flames as illustrated in Figure 6.

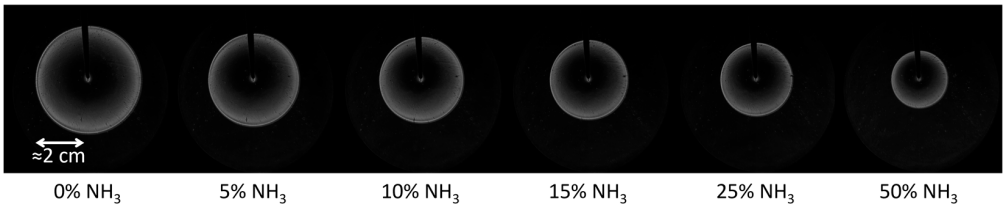

Figure 5. Examples of biogas/NH_3/air flame images at ϕ = 1, P = 1 bar, and T = 300 ± 3 K, 16 ms after the spark.

In Figure 7, S_L^0 is plotted over the equivalence ratio for various biogas/ammonia blends with ammonia content ranging from 0 to 50%vol. in the fuel mixture. The pure ammonia results are taken from [15]. As expected, adding ammonia to the fuel mixture decreases the laminar flame speed towards the value of pure ammonia. The flame speed shows a non-linear decrease with the first important step only with a 5% ammonia addition. Results present higher uncertainties on the rich side, at ϕ = 1.2, with the 10% NH_3 blend showing a lower value than the 15% one which is due to the experimental uncertainty. This higher uncertainty is mainly due to a higher standard deviation on the flame speed value. This can be caused by two reasons: a higher stretch sensitivity that makes the laminar flame speed

extrapolation more difficult to fit, and/or some instabilities that can occur, as shown in Figure 6, thus shortening the radius range for the flame speed extrapolation and increasing the standard deviation on the unstretched flame speed. On top of that, the 5% blend condition $\phi = 1.2$ seems low, whereas for the 25% blend, it seems, at the same equivalence ratio, slightly too high. Globally, the two selected mechanisms capture the experimental results well, with the Okafor mechanism performing better than CEU-NH3-Mech-1.1 on the lean side and vice versa on the rich side.

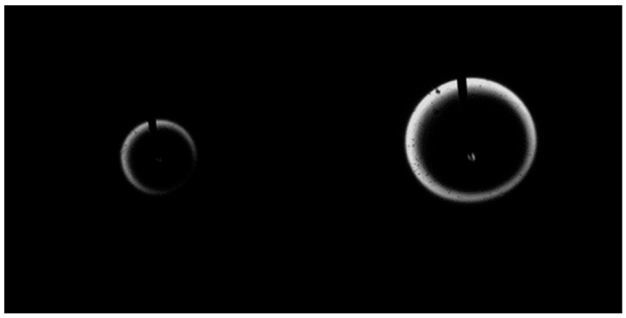

Figure 6. Example of biogas/NH_3/air flame images for 75% of NH_3, at ϕ = 1.1, P = 1 bar, and T = 300 ± 3 K, 16 ms (**left**) and 44 ms (**right**) after the spark, showing first an extinction and then strong buoyancy effect. The exposure time was increased compared to Figure 5 for better visualization.

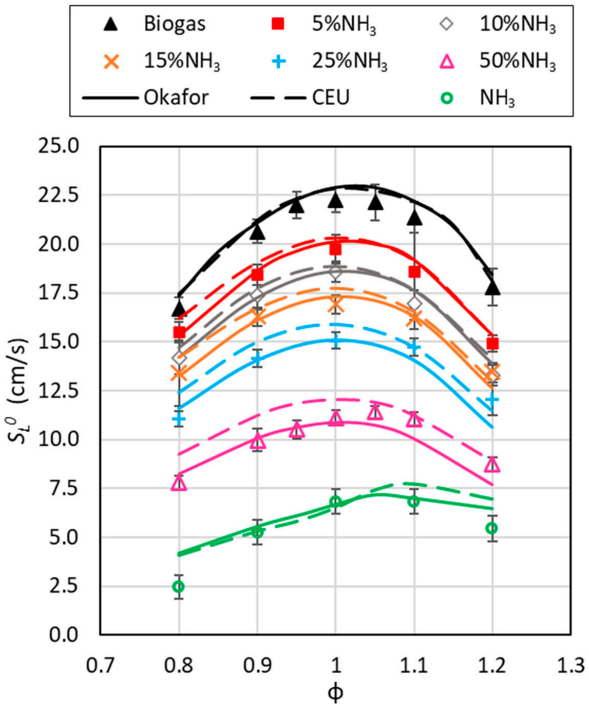

Figure 7. Experimental and numerical laminar flame speed vs. equivalence ratio for various biogas/NH_3 blends. P = 1 bar; T = 300 ± 3 K. Pure ammonia data were taken from [15]. All data are available in the Table S1 of the Supplementary Material.

3.3. Markstein Lengths

The Markstein lengths, obtained by the non-linear extrapolation model (Equation (3)), are displayed as a function of the equivalence ratio for all the studied blends in Figure 8. The Markstein lengths of pure ammonia extracted from [15] are presented for comparison. Globally, in terms of stretch sensitivity, the biogas/ammonia blends behave similarly to pure biogas. Yet, it can be noted that adding NH_3 to the blend leads to a Markstein length increase especially on the rich side. The upper (and lower) error bars for neat ammonia

taken from Zitouni et al. [15] represent the difference between the maximum (and minimum, respectively) values determined against the average Markstein length. For biogas and blends with NH_3, no error bar is plotted for the sake of clarity, but the standard deviation over three consecutive tests is generally around 5% and never exceeds 15% which is obtained for the leanest case, where the measurement is the most difficult. In conclusion, it can be said that up to 50% of NH_3, the flame response to the flame stretch of the biogas/NH_3 blend is very similar to that of the biogas flame, at least for near-stoichiometric mixture thus probably not affecting that much the operation of a biogas system with NH_3 addition. A relationship between the Markstein length and other fundamental parameters such as Lewis and Zel'dovich based on spherically expanding flames was derived by Chen [29] from analytical development as follows:

$$L_b = \left[\frac{1}{Le} - \left(\frac{Ze}{2}\right)\left(\frac{1}{Le} - 1\right)\right].\frac{\rho_b}{\rho_u}\delta_k \quad (4)$$

where Le is the Lewis number, defined as the thermal diffusivity to the mass diffusivity, Ze, the Zel'dovich number, and δ_k the kinetic flame thickness defined as $\delta_k = \lambda/\left(\rho_u.c_p.S_L^0\right)$ where λ represents the thermal conductivity and c_p the specific heat at constant pressure. This relationship was further used by Bouvet et al. [30], Lapalme et al. [25] and Zitouni et al. [31]. Adding ammonia to biogas will affect each of these parameters: it will increase the flame thickness (along with a decrease in the flame speed), and the Zel'dovich number will also increase, as the activation energy is much higher for neat ammonia [15]. Last, the diffusion properties of biogas/air could be modified by the addition of ammonia. Vieira et al. [32] showed that first CO_2 dilution does not affect the methane/air Lewis number on the lean side and decreases it moderately on the rich side. In addition, Zitouni et al. [15] showed that adding ammonia to methane does not affect the Lewis number of the blend: it slightly decreases for lean and stoichiometric mixtures, and does not change it for rich mixtures. Consequently, the moderate change in the Markstein length observed when mixing ammonia and biogas (up to 50%vol. NH_3), seems to be related to flame thickness and Zel'dovich changes rather than to a modification of the diffusive properties of the blend through the Lewis number.

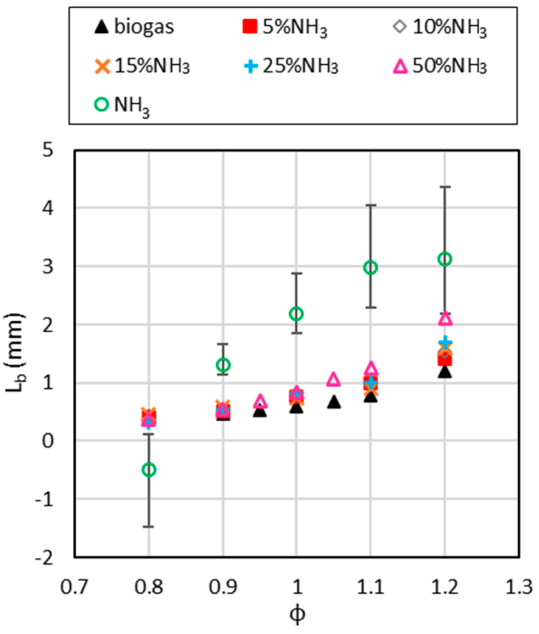

Figure 8. Experimental Markstein lengths vs. equivalence ratio for various biogas/NH_3 blends. P = 1 bar; T = 300 ± 3 K. Pure ammonia data taken from [15]. All data are available in the Table S1 of the Supplementary Material.

3.4. Radiative Heat Losses

Regarding the radiative heat losses, it is well known that CO_2 and NH_3 can be important contributors. In order to assess this impact, the optically thin model (OTM) implemented in ANSYS CHEMKIN-PRO was used. In ANSYS CHEMKIN-PRO, the radiative heat loss from a mixture of gases is given by the optically thin model through:

$$\dot{Q_{rad}} = 4\sigma \left[\left(T^4 - T_{amb}^4 \right) \sum_i P(X_i a_i) \right] \quad (5)$$

where σ is the Stefan-Boltzmann constant, T is the gas temperature, T_{amb} is the ambient temperature, P is the gas pressure, X_i the mole fraction of species i, and a_i is the Planck mean absorption coefficient. The Planck absorption coefficients are directly taken from the thermodynamic data file of the CEU-NH3-Mech-1.1 provided by Wang et al. [21]. It should be noted that this type of radiation model does not account for the reabsorption of heat loss in the burnt gases by the fresh gases thus usually overestimating radiative effects [33]. In the present case, where CO_2 is both present in the burned and fresh gases, this could be of importance. Therefore, the results obtained from the OTM are compared with the correlation of Yu et al. [34], which is based on the statistical narrow band model (SNB), calculated as follows:

$$\frac{S_{L radiative}^0}{S_{L adiabatic}^0} = 1 - 0.82 \left(\frac{S_{L adiabatic}^0}{S_0} \right)^{-1.14}, \quad (6)$$

where $S_0 = 1$ cm/s. This correlation should therefore consider reabsorption, but it was only validated on H_2/CO blends, CH_4, C_3H_8 and C_8H_{18} and does not work for diluted mixtures with a high content of CO_2 (important reabsorption) thus probably leading to an overestimation of the radiative effect as highlighted by Yu et al. [34]. Indeed, Yu et al. showed that for a 6% dilution with CO_2 of a stoichiometric CH_4/air (which corresponds to the 60/40 biogas composition), the radiation-induced error on the flame speed stays below 2% at ambient conditions. Since the radiation effect is the most critical at low speeds, results are presented for the leanest/richest case in Figure 9a and b respectively. Based on previous comparisons, Okafor/CEU-NH3-Mech-1.1 mechanisms were used for the lean/rich cases respectively. Globally, results show that considering radiation either with the OTM or with the Yu et al. correlation leads to a decrease in the flame speed compared to the adiabatic case. Globally, the simulated flame speeds accounting for radiation agree better with the experimental results, but it should be highlighted that both simulations (adiabatic and radiative) and the correlation fall within the uncertainty bars of the experimental data. Higher discrepancies are visible on the rich side, as already seen in Figure 7, mainly because of higher uncertainties on the quantity of ammonia. Moreover, as explained by Chen et al. [33], the OTM usually overestimates the heat losses caused by radiation since it does not consider reabsorption. The correlation of Yu et al. behaves similarly for CO_2 diluted mixtures: it overestimates the decrease of the flame speed according to its authors [34]. As a result, it is possible that experimentally, the reabsorption by the fresh gases compensates for the heat losses in burnt gases resulting in evolutions almost similar to an adiabatic case. Plotting both the adiabatic and the OTM cases already shows the boundaries of possible flame speed values and the maximum difference between them. As a result, the present flame speed measurements for the biogas/NH_3/air mixture seem to be not that much affected by radiation, at least for blends with less than 25% vol. of NH_3. For 50%vol. of NH_3, the relative difference between adiabatic and radiation-affected case is about 5 and 8% for the rich and lean cases respectively.

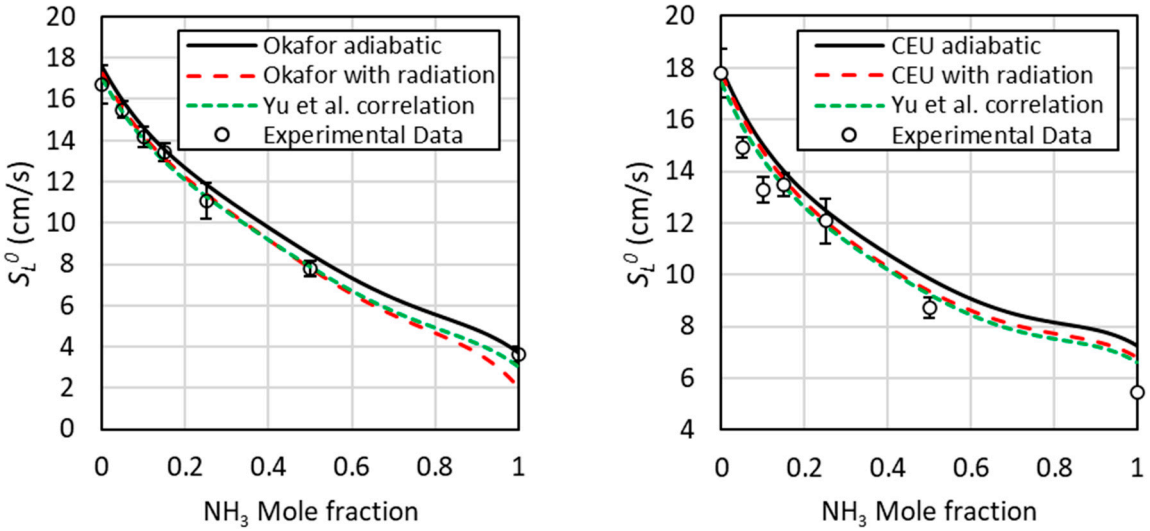

(**a**) (**b**)

Figure 9. Laminar flame speed vs. NH_3 amount calculated with and without radiation using OTM and Yu et al. correlation [34] compared with experimental data at 1 bar; 300 K (**a**) ϕ = 0.8; (**b**) ϕ = 1.2.

4. Conclusions

In this study, first data for laminar flame speeds and Markstein lengths of biogas/ammonia blends are presented (to the best of the authors knowledge). For biogas only, results are in good agreement with the literature and kinetic mechanisms. Adding ammonia to the blend decreases the laminar flame speed due to the low reactivity of NH_3. In terms of Markstein lengths, the blends present a similar stretch sensitivity as pure biogas. Yet an increase in the Markstein length is noticeable on the rich side with the ammonia addition. The measurements were limited to blends below 50%vol. of NH3 due to the occurrence of local quasi-extinction and buoyancy instabilities. Okafor et al. and CEU-NH3-Mech-1.1 kinetics mechanism show good agreement with the experimental data with, respectively, about 5 and 7% differences on average with all experimental data. A first attempt to assess the uncertainty related to radiative heat losses was conducted, showing a very limited impact on the results, at least for biogas/NH_3 with less than 50% vol. of NH_3.

Supplementary Materials: The following supporting information can be downloaded at: https://www.mdpi.com/article/10.3390/en17020319/s1, Table S1: experimental database for laminar burning velocities and Markstein lengths.

Author Contributions: Conceptualization, P.B. and A.S.; methodology, P.B.; validation, P.B., C.M.-R., F.H. and G.D.; formal analysis, P.B. and A.S.; investigation, P.B. and A.S.; data curation, P.B. and A.S.; writing—original draft preparation, P.B.; writing—review and editing, P.B., C.M.-R., F.H. and G.D.; supervision, P.B., C.M.-R., F.H. and G.D.; funding acquisition, P.B. All authors have read and agreed to the published version of the manuscript.

Funding: The research leading to these results has received funding from the CNRS through PEPS Energie 2022 program: project MASYNBIOZ. The authors also thank CNRS/FITe (FR2039): Fédération pour l'Innovation et la Transition énergétique for its financial support.

Data Availability Statement: The original contributions presented in the study are included in the article/Supplementary Material, further inquiries can be directed to the corresponding author.

Acknowledgments: The authors are grateful to their students Gauthier Brienne and Alexandre Guillemot, for their technical support during the experimental campaign.

Conflicts of Interest: The authors declare no conflict of interest. The funders had no role in the design of the study; in the collection, analyses, or interpretation of data; in the writing of the manuscript; or in the decision to publish the results.

References

1. Scarlat, N.; Dallemand, J.; Taylor, N.; Banja, M. *Brief on Biomass for Energy in the European Union*; Publications Office of the European Union: Luxembourg, 2019; pp. 1–8.
2. Calbry-Muzyka, A.; Madi, H.; Rüsch-Pfund, F.; Gandiglio, M.; Biollaz, S. Biogas Composition from Agricultural Sources and Organic Fraction of Municipal Solid Waste. *Renew. Energy* **2022**, *181*, 1000–1007. [CrossRef]
3. Wagner, A.O.; Hohlbrugger, P.; Lins, P.; Illmer, P. Effects of Different Nitrogen Sources on the Biogas Production—A Lab-Scale Investigation. *Microbiol. Res.* **2012**, *167*, 630–636. [CrossRef] [PubMed]
4. Feiz, R.; Johansson, M.; Lindkvist, E.; Moestedt, J.; Påledal, S.N.; Svensson, N. Key Performance Indicators for Biogas Production—Methodological Insights on the Life-Cycle Analysis of Biogas Production from Source-Separated Food Waste. *Energy* **2020**, *200*, 117462. [CrossRef]
5. Lhuillier, C.; Brequigny, P.; Lamoureux, N.; Contino, F.; Mounaïm-Rousselle, C. Experimental Investigation on Laminar Burning Velocities of Ammonia/Hydrogen/Air Mixtures at Elevated Temperatures. *Fuel* **2020**, *263*, 116653. [CrossRef]
6. Grannell, S.M.; Assanis, D.N.; Bohac, S.V.; Gillespie, D.E. The Fuel Mix Limits and Efficiency of a Stoichiometric, Ammonia, and Gasoline Dual Fueled Spark Ignition Engine. *J. Eng. Gas Turbines Power* **2008**, *130*, 042802. [CrossRef]
7. Mørch, C.S.; Bjerre, A.; Gøttrup, M.P.; Sorenson, S.C.; Schramm, J. Ammonia/Hydrogen Mixtures in an SI-Engine: Engine Performance and Analysis of a Proposed Fuel System. *Fuel* **2011**, *90*, 854–864. [CrossRef]
8. Westlye, F.R.; Ivarsson, A.; Schramm, J. Experimental Investigation of Nitrogen Based Emissions from an Ammonia Fueled SI-Engine. *Fuel* **2013**, *111*, 239–247. [CrossRef]
9. Koch, E. Ammonia as a Fuel for Motor Buses. *J. Inst. Pet.* **1949**, *31*, 21–32.
10. Nonaka, H.O.B.; Pereira, F.M. Experimental and Numerical Study of CO_2 Content Effects on the Laminar Burning Velocity of Biogas. *Fuel* **2016**, *182*, 382–390. [CrossRef]
11. Hinton, N.; Stone, R. Laminar Burning Velocity Measurements of Methane and Carbon Dioxide Mixtures (Biogas) over Wide Ranging Temperatures and Pressures. *Fuel* **2014**, *116*, 743–750. [CrossRef]
12. Wei, Z.; Zhen, H.; Fu, J.; Leung, C.; Cheung, C.; Huang, Z. Experimental and Numerical Study on the Laminar Burning Velocity of Hydrogen Enriched Biogas Mixture. *Int. J. Hydrogen Energy* **2019**, *44*, 22240–22249. [CrossRef]
13. Hayakawa, A.; Goto, T.; Mimoto, R.; Arakawa, Y.; Kudo, T.; Kobayashi, H. Laminar Burning Velocity and Markstein Length of Ammonia/Air Premixed Flames at Various Pressures. *Fuel* **2015**, *159*, 98–106. [CrossRef]
14. Kanoshima, R.; Hayakawa, A.; Kudo, T.; Okafor, E.C.; Colson, S.; Ichikawa, A.; Kudo, T.; Kobayashi, H. Effects of Initial Mixture Temperature and Pressure on Laminar Burning Velocity and Markstein Length of Ammonia/Air Premixed Laminar Flames. *Fuel* **2022**, *310*, 122149. [CrossRef]
15. Zitouni, S.-E.; Brequigny, P.; Mounaïm-Rousselle, C. Influence of Hydrogen and Methane Addition in Laminar Ammonia Premixed Flame on Burning Velocity, Lewis Number and Markstein Length. *Combust. Flame* **2023**, *253*, 112786. [CrossRef]
16. Mong, G.R.; Chiong, M.-C.; Chong, C.T.; Ng, J.-H.; Mashruk, S.; Tran, M.-V.; Lee, K.M.; Samiran, N.A.; Wong, K.Y.; Valera-Medina, A. Fuel-Lean Ammonia/Biogas Combustion Characteristics under the Reacting Swirl Flow Conditions. *Fuel* **2023**, *331*, 125983. [CrossRef]
17. Shu, T.; Xue, Y.; Zhou, Z.; Ren, Z. An Experimental Study of Laminar Ammonia/Methane/Air Premixed Flames Using Expanding Spherical Flames. *Fuel* **2021**, *290*, 120003. [CrossRef]
18. Okafor, E.C.; Naito, Y.; Colson, S.; Ichikawa, A.; Kudo, T.; Hayakawa, A.; Kobayashi, H. Experimental and Numerical Study of the Laminar Burning Velocity of CH_4–NH_3–Air Premixed Flames. *Combust. Flame* **2018**, *187*, 185–198. [CrossRef]
19. Okafor, E.C.; Naito, Y.; Colson, S.; Ichikawa, A.; Kudo, T.; Hayakawa, A.; Kobayashi, H. Measurement and Modelling of the Laminar Burning Velocity of Methane-Ammonia-Air Flames at High Pressures Using a Reduced Reaction Mechanism. *Combust. Flame* **2019**, *204*, 162–175. [CrossRef]
20. Han, X.; Wang, Z.; Costa, M.; Sun, Z.; He, Y.; Cen, K. Experimental and Kinetic Modeling Study of Laminar Burning Velocities of NH_3/Air, NH_3/H_2/Air, NH_3/CO/Air and NH_3/CH_4/Air Premixed Flames. *Combust. Flame* **2019**, *206*, 214–226. [CrossRef]
21. Wang, S.; Wang, Z.; Chen, C.; Elbaz, A.M.; Sun, Z.; Roberts, W.L. Applying Heat Flux Method to Laminar Burning Velocity Measurements of NH_3/CH_4/Air at Elevated Pressures and Kinetic Modeling Study. *Combust. Flame* **2022**, *236*, 111788. [CrossRef]
22. Moffat, R.J. Describing the Uncertainties in Experimental Results. *Exp. Therm. Fluid Sci.* **1988**, *1*, 3–17. [CrossRef]
23. Chi, C.; Han, W.; Thévenin, D. Effects of Molecular Diffusion Modeling on Turbulent Premixed NH_3/H_2/Air Flames. *Proc. Combust. Inst.* **2022**, *17*, 1–10. [CrossRef]
24. Ben Zenou, J.; Vicquelin, R. Acceleration of Premixed H_2-Air-Steam Flames When Accounting for Thermal Radiation. *Combust. Flame* **2023**, *258*, 113068. [CrossRef]
25. Lapalme, D.; Halter, F.; Mounaïm-Rousselle, C.; Seers, P. Characterization of Thermodiffusive and Hydrodynamic Mechanisms on the Cellular Instability of Syngas Fuel Blended with CH_4 or CO_2. *Combust. Flame* **2018**, *193*, 481–490. [CrossRef]
26. Shrestha, K.P.; Seidel, L.; Zeuch, T.; Mauss, F. Detailed Kinetic Mechanism for the Oxidation of Ammonia Including the Formation and Reduction of Nitrogen Oxides. *Energy Fuels* **2018**, *32*, 10202–10217. [CrossRef]
27. University of California at San Diego Chemical-Kinetic Mechanisms for Combustion Applications", San Diego Mechanism Web Page. Available online: http://web.eng.ucsd.edu/mae/groups/combustion/mechanism.html (accessed on 27 November 2023).
28. Nurmukan, D.; Chen, T.J.M.; Hung, Y.M.; Ismadi, M.Z.; Chong, C.T.; Tran, M.V. Enhancement of Biogas/Air Combustion by Hydrogen Addition at Elevated Temperatures. *Int. J. Energy Res.* **2020**, *44*, 1519–1534. [CrossRef]

29. Chen, Z. On the Extraction of Laminar Flame Speed and Markstein Length from Outwardly Propagating Spherical Flames. *Combust. Flame* **2011**, *158*, 291–300. [CrossRef]
30. Bouvet, N.; Halter, F.; Chauveau, C.; Yoon, Y. On the Effective Lewis Number Formulations for Lean Hydrogen/Hydrocarbon/Air Mixtures. *Int. J. Hydrogen Energy* **2013**, *38*, 5949–5960. [CrossRef]
31. Zitouni, S.; Pugh, D.; Crayford, A.; Bowen, P.J.; Runyon, J. Lewis Number Effects on Lean Premixed Combustion Characteristics of Multi-Component Fuel Blends. *Combust. Flame* **2022**, *238*, 111932. [CrossRef]
32. Vieira, M.C.d.J.; Figueira da Silva, L.F. Flame Flashback Critical Damköhler Number for CO_2 Diluted CH_4 and C_3H_8 Mixtures with Air. *Flow, Turbul. Combust.* **2023**, *110*, 377–393. [CrossRef]
33. Chen, Z.; Qin, X.; Xu, B.; Ju, Y.; Liu, F. Studies of Radiation Absorption on Flame Speed and Flammability Limit of CO_2 Diluted Methane Flames at Elevated Pressures. *Proc. Combust. Inst.* **2007**, *31*, 2693–2700. [CrossRef]
34. Yu, H.; Han, W.; Santner, J.; Gou, X.; Sohn, C.H.; Ju, Y.; Chen, Z. Radiation-Induced Uncertainty in Laminar Flame Speed Measured from Propagating Spherical Flames. *Combust. Flame* **2014**, *161*, 2815–2824. [CrossRef]